

# Supporting Information

## Improving the Performance of Supported Ionic Liquid Phase (SILP) Catalysts for the Ultra-Low-Temperature Water-Gas Shift Reaction Using Organic Salt Additives

Patrick Wolf<sup>1,2‡</sup>, Christian R. Wick<sup>3,4‡</sup>, Julian Mehler<sup>1</sup>, Dominik Blaumeiser<sup>5</sup>, Simon Schötz<sup>5</sup>, Tanja Bauer<sup>5</sup>, Jörg Libuda<sup>5</sup>, David Smith<sup>6</sup>, Ana-Sunčana Smith<sup>3,6</sup>, Marco Haumann<sup>1\*</sup>

<sup>1</sup>Friedrich-Alexander-Universität Erlangen-Nürnberg (FAU), Lehrstuhl für Chemische Reaktionstechnik (CRT), Egerlandstr. 3, 91058, Erlangen, Germany

<sup>2</sup>Forschungszentrum Jülich GmbH, Helmholtz Institute Erlangen-Nürnberg for Renewable Energy (IEK-11), Cauerstraße 1, 91058 Erlangen, Germany

<sup>3</sup>PULS Group, Institute for Theoretical Physics and Interdisciplinary Center for Nanostructured Films (IZNF), Friedrich-Alexander-Universität Erlangen-Nürnberg, Cauerstraße 3, 91058, Erlangen, Germany

<sup>4</sup>Competence Unit for Scientific Computing (CSC), Friedrich-Alexander-Universität Erlangen-Nürnberg, Martensstrasse 5a, 91058, Erlangen, Germany

<sup>5</sup>Interface Research and Catalysis, Erlangen Center for Interface Research and Catalysis, Friedrich-Alexander-Universität Erlangen-Nürnberg, Egerlandstraße 3, D-91058 Erlangen, Germany

<sup>6</sup>Group of Computational Life Sciences, Department of Physical Chemistry, Ruđer Bošković Institute, Bijenička 54, 10000 Zagreb, Croatia

‡ both authors contributed equally to the work

Corresponding author: marco.haumann@fau.de

## Preparation of SILP catalysts with different additives

First, the IL  $[C_4C_1C_1Im]Cl$  (Merck KgaA, LOT: 99/818) was dissolved in 15 mL of dichloromethane (DCM; Sigma-Aldrich, LOT: SZBG073AV) and stirred for 10 - 15 min. Second, the ruthenium dimer precursor  $[Ru(CO)_2Cl_3]_2$  (Alfa Aesar, LOT: X06C034, purity: > 98%) was added using further DCM and stirred for another 10 - 15 min. Subsequently, the additive (methylene blue (MB), Acros Organics LOT:A0388231; methylene green (MG), MP Biomedicals LOT: Q9173; thionine chloride, abcr GmbH LOT: 1024719; azure A, abcr GmbH LOT: 1400053; 2,2'-bipyridine, Merck KgaA LOT: D216305; 1,10-phenanthroline, Merck KgaA LOT: 131377; acridine orange, Acros Organics LOT:A0395196; brilliant cresyl blue, PanReac AppliChem LOT:0001436355; neutral red, Acros Organics LOT: A0396749), dissolved in 20 mL of DCM, was added and the mixture was stirred for an additional 60 – 90 min. Last, the alumina support ( $\gamma$ - $Al_2O_3$ , Sasol Germany GmbH, LOT: B39598) was added to the mixture and stirred no longer than 2 – 5 min to avoid mechanical stress of the support material. The solvent was slowly removed under reduced pressure. The free-flowing SILP catalyst powder was stored under an argon atmosphere. The Ru-loading of the SILP catalyst was  $w_{Ru} = 0.02 \text{ g}_{Ru} \text{ g}_{support}^{-1}$ . The pore filling grade of the support, which describes the IL volume related to the total pore volume of the support material ( $V_{IL} V_{support}^{-1}$ ), was  $\alpha = 0.34$ . The molar amount of additive related to the IL (in  $\text{mol L}_{IL}^{-1}$ ) was varied between 0.25 M and 2 M, corresponding to a molar ratio  $\chi$  (in  $\text{mol}_{additive} / \text{mol}_{IL}$ ) of 0.04 – 0.35, respectively.

## Synthesis of methylene blue with hydrogen sulfate as anion (MB-HSO<sub>4</sub>)

An aqueous solution of methylene blue (31.3 mM) was treated with an Amberlite IRN-78 anion exchange resin, to give a solution of [MB-OH] (2 L, 13.1 mM), which was subsequently neutralized with 1 eq. of H<sub>2</sub>SO<sub>4</sub>. H<sub>2</sub>O was removed under reduced pressure and the remaining residue was further dried *in vacuo*. The product was obtained as a dark-blue solid (10.15 g, 26.2 mmol, 83.7 %) and tested negative for Cl<sup>-</sup> with AgNO<sub>3</sub>.

## Continuous gas-phase reactor setup

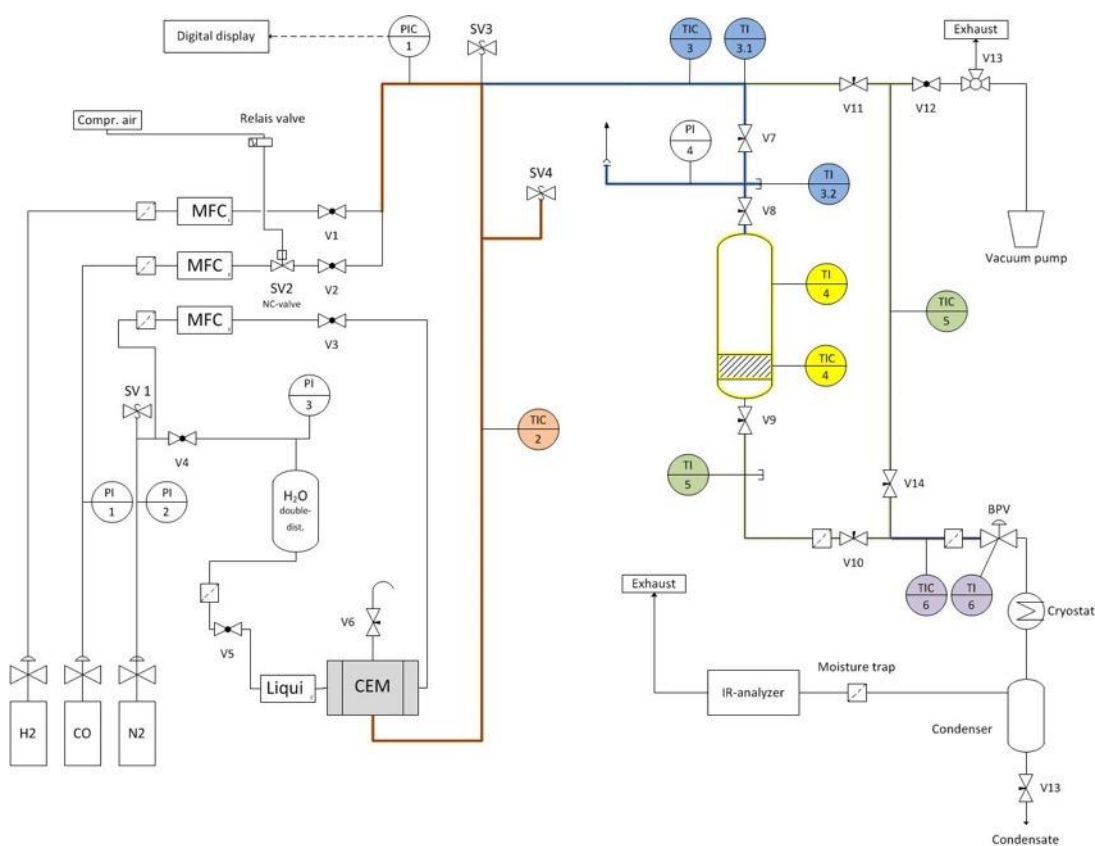


**Figure S1.** Flow scheme of the continuous fixed-bed reactor for the catalytic evaluation of the different samples. Red: gas dosing and mixing section, blue: upstream section, yellow: fixed-bed reactor, green: downstream/bypass section, purple: pressure regulation.

## Evaluation of catalytic experiments

After the ramp-up phase under a low  $N_2$  flow ( $50 \text{ mL}_N \text{ min}^{-1}$ ), the reaction mixture was directed through the bypass-line in order to gain a reference point for the calculation of the catalytic activity. Subsequently, the gas stream was sent through the fixed-bed reactor and an automated temperature variation program was started (temperature variation from  $120^\circ\text{C}$  as reference set point to  $140^\circ\text{C}$  in  $5^\circ\text{C}$  steps with a reference set point in-between each temperature). Every temperature stage was kept for 5 h, so that a total time-on-stream (TOS) of 45 h was reached. The results of such a typical characterization experiment can be seen for example in Figure S2 for both the benchmark and methylene blue (MB) modified SILP catalyst.

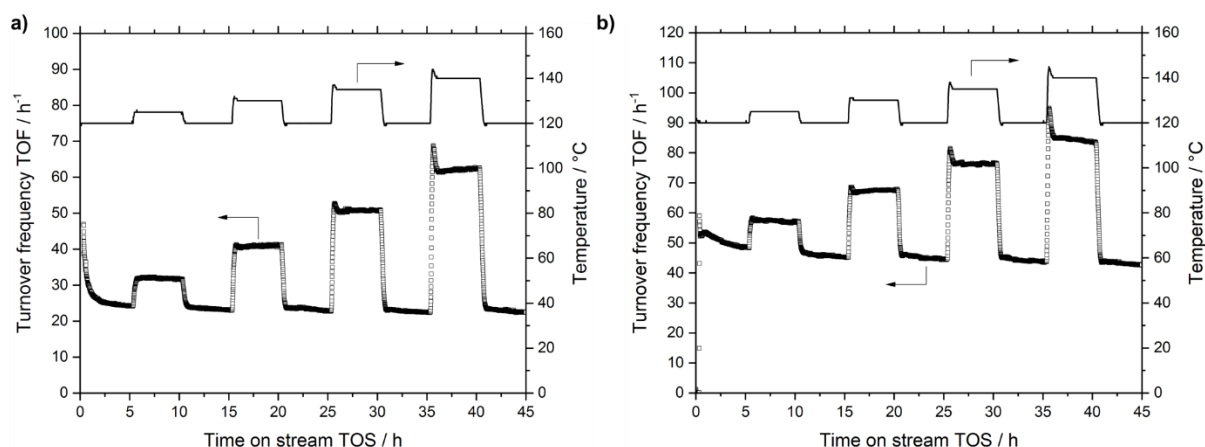


**Figure S2.** Turnover frequency (TOF) data obtained from a) benchmark and b) methylene blue modified SILP WGS catalyst sample. TOF (left y-axis) and temperature in the catalyst bed (right y-axis) are plotted over time-on-stream (TOS) of the continuous experiment.  $T = 120 - 140^\circ\text{C}$ ,  $p = 1 \text{ bar}$ , precursor =  $[\text{Ru}(\text{CO})_3(\text{Cl})_2]_2$ , loading (Ru) =  $0.02 \text{ g g}_{\text{Support}}^{-1}$ , IL =  $[\text{C}_4\text{C}_1\text{C}_1\text{Im}]\text{Cl}$ ,  $\alpha = 0.34$ ,  $m_{\text{cat}} = 2.0 \text{ g}$ ,  $p_{\text{H}_2\text{O}}:p_{\text{CO}} = 2:1$ ,  $\dot{V}_{\text{tot}} = 174 \text{ mL}_N \text{ min}^{-1}$ , TOS = 45 h.

As a measure for the catalytic activity, the Ru-based turnover frequency (TOF) has been calculated for every system. The basis for the evaluation is a temperature variation experiment at constant feed flows and compositions. Using the example of a benchmark catalyst (BM), the result of a

typical experiment is shown in Figure S1. Turnover frequency (TOF) values are plotted as a function of the reaction temperature versus time-on-stream of the continuous catalytic experiment demonstrating good stability of the system after a short ramp-up phase.

Since the amount of additive can be related to the fixed amount of IL, which is basically determined by the pore volume of the support material and the pore filling grade, it is given as molarity value M. For the sake of clarity, the conversion between molarities and the molar ratio of additive to IL  $\chi$  is given in Table S1. Additionally, the molar ratio of additive to ruthenium  $\xi$  is listed as well.

**Table S1.** Conversion between molarities of the additive (M) and molar ratio of additive to IL ( $\chi$ ). Additionally, the molar ratio of the additive to ruthenium ( $\xi$ ) is given.

<b>Molarity M</b> <b>mol<sub>additive</sub> L<sub>IL</sub><sup>-1</sup></b>	<b>Additive to IL ratio <math>\chi</math></b> <b>mol<sub>additive</sub> mol<sub>IL</sub><sup>-1</sup></b>	<b>Additive to Ru ratio <math>\xi</math></b> <b>mol<sub>additive</sub> mol<sub>Ru</sub><sup>-1</sup></b>
0.00	0.000	0.000
0.25	0.043	0.191
0.50	0.087	0.385
0.75	0.130	0.578
1.00	0.174	0.771
1.50	0.261	1.156
2.00	0.348	1.542

For each additive experiment in all subsequent Figures, 2.0 g of catalyst (molarity of the additive is given in the respective caption) was placed in the reactor and tested in a temperature variation experiment (120 °C – 140 °C in 5 °C steps) with a total TOS of 45 h.

### Comparison of ATR spectra of SILP and freshly prepared mixture

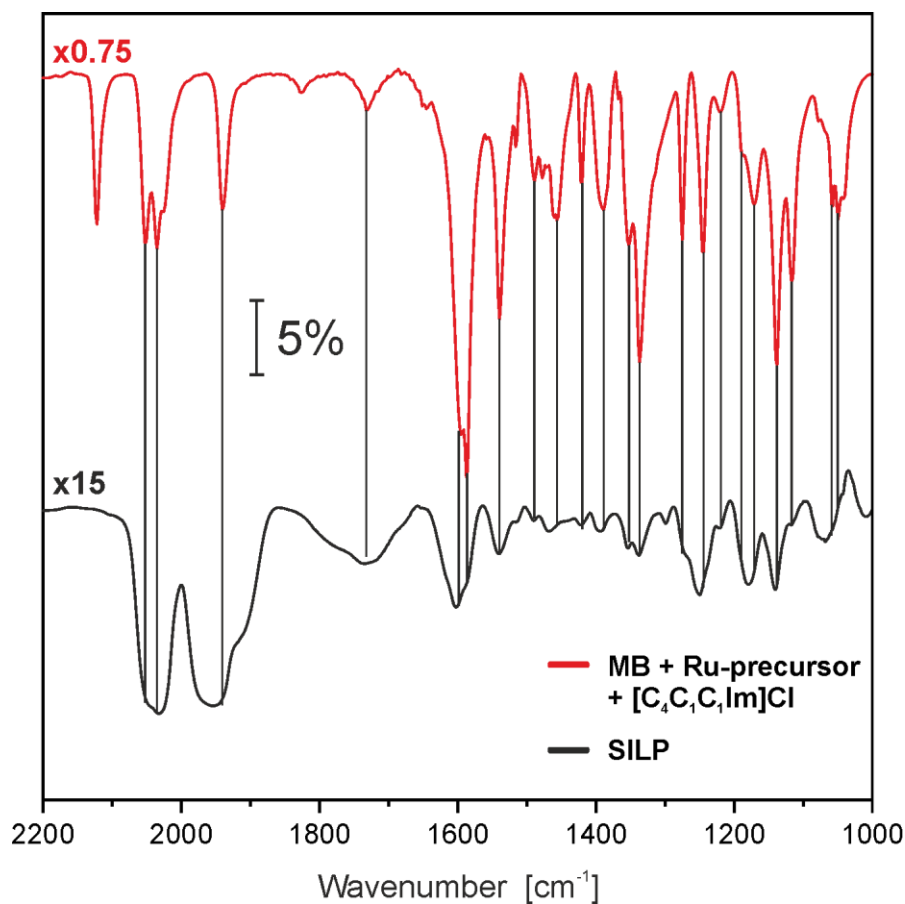


**Figure S3.** IR spectra of a Ru-based SILP system and the corresponding freshly prepared mixture.

In Figure S3, a comparison is shown between the Ru-based SILP system and the corresponding freshly prepared mixture of MB, the  $[\text{Ru}(\text{CO})_3\text{Cl}_2]_2$  precursor, and  $[\text{C}_4\text{C}_1\text{C}_1\text{Im}]\text{Cl}$ . Note that these samples only differ in the fact that the SILP system is supported on  $\text{Al}_2\text{O}_3$ . The peak positions in Figure S3 are extended to demonstrate that the peak positions of the two samples are identical. Note that there are two differences: On the one hand, the CO region shows different peaks. This is due to dimer splitting of the  $[\text{Ru}(\text{CO})_3\text{Cl}_2]_2$  precursor as compared to the freshly prepared mixture.

On the other hand, the peaks in the ATR spectrum of the SILP system are broader as compared to the freshly prepared mixture. In consequence, the investigation of the freshly prepared mixture of MB, the  $[\text{Ru}(\text{CO})_3\text{Cl}_2]_2$  precursor, and  $[\text{C}_4\text{C}_1\text{C}_1\text{Im}]\text{Cl}$  serves as a valid system to investigate the Ru-based system applied in the catalytic tests. This is supported by the higher spectral resolution of the peaks in the ATR spectrum of the mixture, which are sharper and more well-defined as compared to the spectrum of the SILP. Thus, small changes are detected more easily.

## Influence of COSMO, CPCM and SMD-GIL implicit solvation on the free Energy of activation.

**Table S2.**  $\Delta\Delta G_{solv}^{\ddagger,298}$  computed at the DLPNO-CCSD(T)/def2TZVPPD // BP86-D3/def2TZVPD level of theory with different solvation models in kJ mol<sup>-1</sup>

	<b>SMD-GIL</b> [C <sub>4</sub> C <sub>1</sub> C <sub>1</sub> Im]Cl	<b>COSMO</b> ( $\epsilon = 12$ )	<b>CPCM</b> ( $\epsilon = 12$ )
<b>benchmark</b>	131.5	121.1	119.9
<b>aniline</b>	146.0	136.4	134.1
<b>N,N-dimethylaniline</b>	117.2	106.9	105.5
<b>N,N-diethylaniline</b>	97.4	92.5	92.1
<b>pyridine</b>	108.7	97.1	95.4
<b>pyrazine</b>	116.6	104.0	102.6
<b>1,4-thiazine</b>	80.0	75.5	74.5
<b>1,4-oxazine</b>	82.5	79.2	78.3
<b>1,4-oxazine-o</b>	128.4	119.5	118.2
<b>4H-1,4-oxazine</b>	128.8	116.5	114.7
<b>4-nitro-pyridine</b>	127.9	120.1	117.9
<b>N,N-dimethylpyridine-4-amine</b>	111.1	98.5	96.8



## Multireference diagnostics

**Table S3.** T1 and Fractional Occupation Number Weighted Density (FOD) multireference diagnostics for the reactions investigated with and without (benchmark) hydrogen bond acceptors.

Complex	N_FOD			T1		
	Reactant	TS	Product	Reactant	TS	Product
1,4-thiazine	0.443	0.524	0.366	0.022	0.020	0.021
aniline	0.283	0.344	0.230	0.021	0.019	0.020
N,N-dimethylaniline	0.302	0.334	0.260	0.021	0.019	0.019
N,N-diethylaniline	0.319	0.332	0.287	0.020	0.018	0.019
pyridine	0.283	0.441	0.281	0.022	0.020	0.020
pyrazine	0.341	0.529	0.333	0.022	0.020	0.020
1,4-oxazine	0.414	0.478	0.308	0.022	0.020	0.021
1,4-oxazine-o	0.337	0.420	0.271	0.022	0.020	0.021
4H-1,4-oxazine	0.393	0.317	0.353	0.022	0.020	0.021
4-nitro-pyridine	0.533	0.809	0.560	0.021	0.020	0.020
N,N-dimethylpyridine- 4-amine	0.288	0.352	0.240	0.021	0.019	0.019
benchmark	0.229	0.247	0.238	0.025	0.023	0.023

## Influence of the chloride ion within MB (anion exchange to MB-HSO<sub>4</sub>)

Due to the fact that MB is a chloride-containing compound, it could be possible that the additional chloride ions introduced into the SILP system via MB are the reason for the vast gain in activity. This theoretical explanation is based on the aforementioned equilibrium between the ruthenium dimer and the active monomeric species,<sup>1</sup> which could be shifted to the side of the monomers upon addition of MB. To investigate whether this effect is responsible for the boost in activity, an anion exchange with MB was conducted. The new anion must not be a halogen ion since the cleavage effect could also take place with other halogens apart from chloride. In order to keep the resulting compound as hydrophilic as the original MB in the chloride version (MB-Cl), hydrogen sulfate was chosen as anion, resulting in MB-HSO<sub>4</sub>.

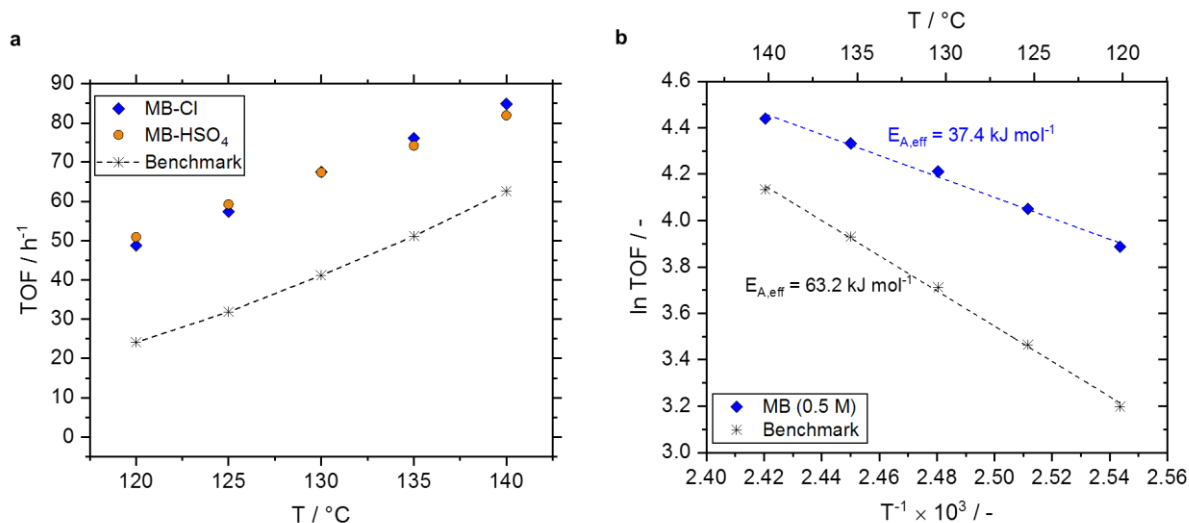


**Figure S4.** Catalytic results (a) for the anion exchanged MB-additive (MB-HSO<sub>4</sub>) compared to the benchmark system (with dashed line) and the original MB version (MB-Cl). Reaction conditions: T = 120 – 140 °C, p = 1 bar, precursor = [Ru(CO)<sub>3</sub>(Cl)<sub>2</sub>]<sub>2</sub>, loading (Ru) = 0.02 g g<sup>-1</sup><sub>Support</sub>, IL = [C<sub>4</sub>C<sub>1</sub>C<sub>1</sub>Im]Cl, α = 0.34, M<sub>additive</sub> = 0.5 mol L<sup>-1</sup>, m<sub>cat</sub> = 2.0 g, p<sub>H<sub>2</sub>O</sub>:p<sub>CO</sub> = 2:1,  $\dot{V}_{tot}$  = 174 mL<sub>N</sub> min<sup>-1</sup>, TOS = 45 h. Maximum error ±5 %, error bars omitted for sake of clarity. Arrhenius plot (b) of steady state activity (TOF) versus inverse temperature. Comparison between benchmark and methylene blue (MB) modified SILP catalyst. Reaction conditions: T = 120 – 140 °C, p = 1 bar, precursor = [Ru(CO)<sub>3</sub>(Cl)<sub>2</sub>]<sub>2</sub>, loading (Ru) = 0.02 g g<sup>-1</sup><sub>Support</sub>, IL = [C<sub>4</sub>C<sub>1</sub>C<sub>1</sub>Im]Cl, α = 0.34, m<sub>cat</sub> = 2.0 g, p<sub>H<sub>2</sub>O</sub>:p<sub>CO</sub> = 2:1,  $\dot{V}_{tot}$  = 174 mL<sub>N</sub> min<sup>-1</sup>, TOS = 45 h.

The experimental results given in Figure S4a reveal that both catalysts, which only differ in the anion of the additive, show almost identical activity values. While the MB-HSO<sub>4</sub> sample is slightly more active at 120 °C (+4 % with regard to MB-Cl), this difference is diminishing with rising temperature. At 130 °C, both systems are equally active. At 140 °C, the MB-Cl catalyst has a TOF, which is 4 % higher than the one obtained with the MB-HSO<sub>4</sub> sample. Based on this experimental data, the hypothesis of the additional free chloride as a reason for the increase in activity is clearly refuted. Hence, the commercially available chloride version of MB (MB-Cl) was used for further investigations. Based on this experimental data, the hypothesis of the additional free chloride as a reason for the increase in activity is clearly refuted. Hence, the commercially available chloride version of MB (MB-Cl) was used for further investigations.

## Concentration variation with MB

Encouraged by the positive effects found for the MB-doped SILP WGS system, we varied the molar ratio  $\chi$  in a set of experiments to investigate a correlation between enhanced catalytic activity and the amount of MB within the catalyst. The results of these concentration variation experiments are summarized in Figure S5 showing an activity versus molar ratio (dopant to IL) plot.

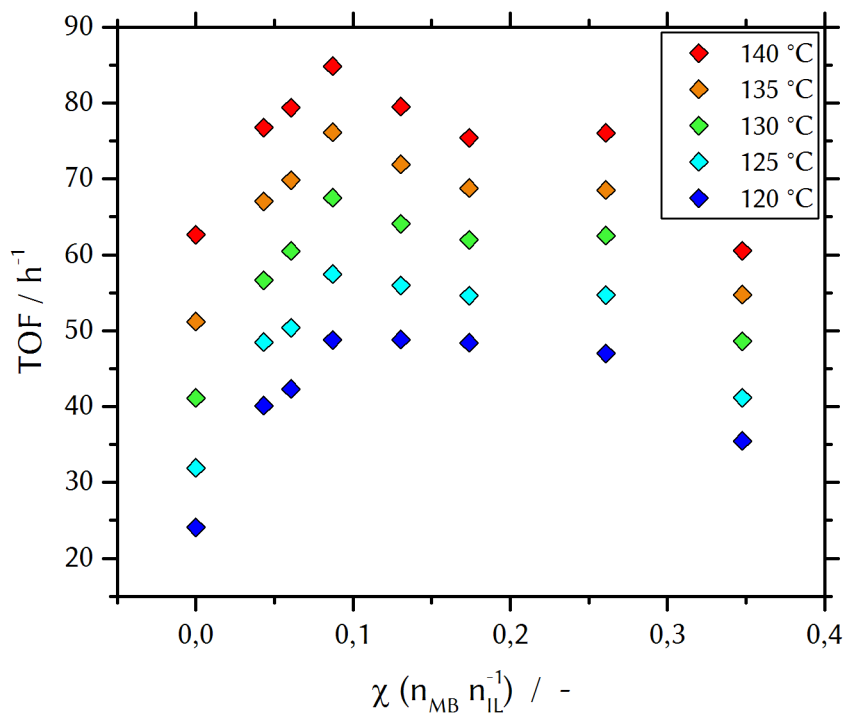
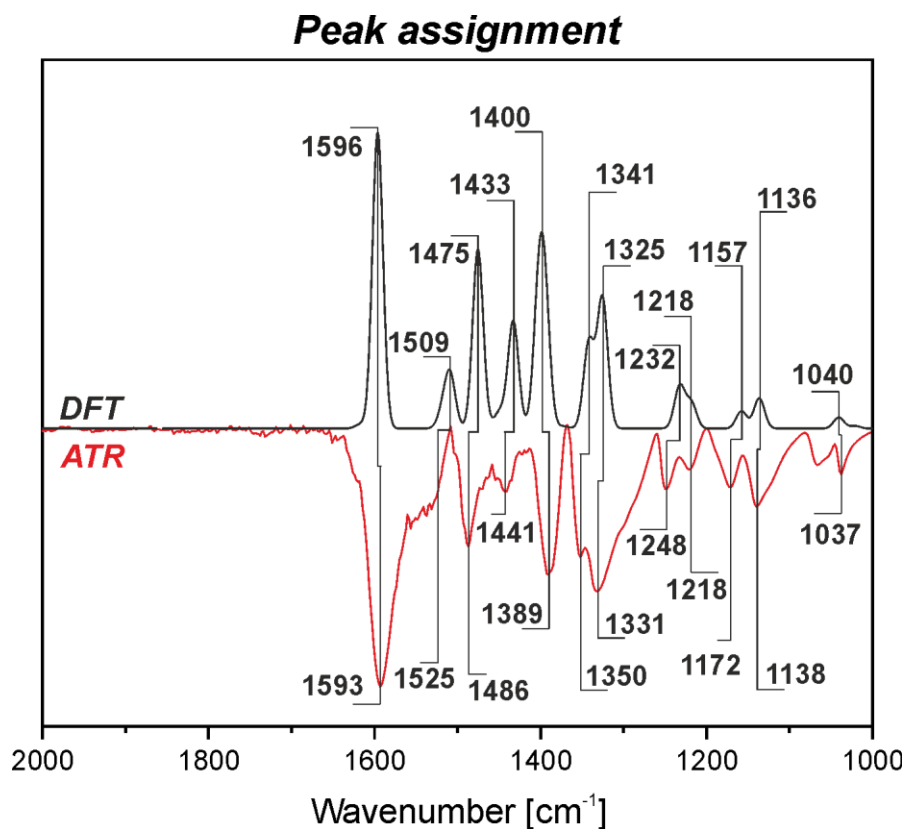


**Figure S5.** Catalytic results for the variation of the MB content in the IL film of the catalyst samples compared to the benchmark system (with dashed line). Reaction conditions:  $T = 120 - 140$  °C,  $p = 1$  bar, precursor =  $[\text{Ru}(\text{CO})_3(\text{Cl})_2]_2$ , loading (Ru) =  $0.02 \text{ g g}_{\text{support}}^{-1}$ , IL =  $[\text{C}_4\text{C}_1\text{C}_1\text{Im}]\text{Cl}$ ,  $\alpha = 0.34$ ,  $M_{\text{MB}} = 0 - 2 \text{ mol L}_{\text{IL}}^{-1}$ ,  $m_{\text{cat}} = 2.0 \text{ g}$ ,  $p_{\text{H}_2\text{O}}:p_{\text{CO}} = 2:1$ ,  $\dot{V}_{\text{tot}} = 174 \text{ mL}_N \text{ min}^{-1}$ , TOS = 45 h. Maximum error  $\pm 5$  %, error bars omitted for sake of clarity.

The experimental data reveals a strong correlation between the MB loading of the IL film and the catalytic activity resulting in a volcano plot-like shape. Already concentrations as small as 0.25 M ( $\chi = 0.043$ ), lead to a significant rise in activity of approximately +67 % (at 120 °C) and +22 % (at

140 °C). Upon further addition of MB, activity rises until a molarity of 0.5 M ( $\chi = 0.087$ ) is reached, representing the peak point of activity in this screening experiment. A higher content of MB shows no significant difference at 120 °C as can be seen upon comparison of the 0.75 M ( $\chi = 0.130$ ) and the 1 M ( $\chi = 0.174$ ) samples. In both cases, the activity boost is still up to +102 % (0.75 M) and +101 % (1 M), respectively. However, the gain in activity of these catalysts becomes less pronounced with rising temperature as compared to the 0.5 M sample with an increase of +27 % (0.75 M) and +20 % (1 M) at 140 °C. Further addition of MB (1.5 M,  $\chi = 0.261$ ) results in slightly negative influences at 120 °C (+95 %). Nevertheless, the 1.5 M catalyst nearly results in the same activity as the 1 M sample (+21 %) at elevated temperatures. Contrary, the 2 M ( $\chi = 0.348$ ) sample shows significantly lower activities of +47 % at 120 °C and even an activity loss compared to the benchmark system of -3 % at 140 °C. The diminishing activity boost upon exceeding a certain concentration of MB could be attributed to its solubility in the IL, so that parts of that additive may be present as a solid. In that way, small pores could be partially blocked with the result that a certain part of the active Ru-species is not accessible anymore for the reactants. Based on the experimental data, the maximum activity boost gained with the lowest amount of MB added is realized with a concentration of 0.5 M. Hence, this molarity value is used for all further investigations.

## Peak assignment of methylene blue

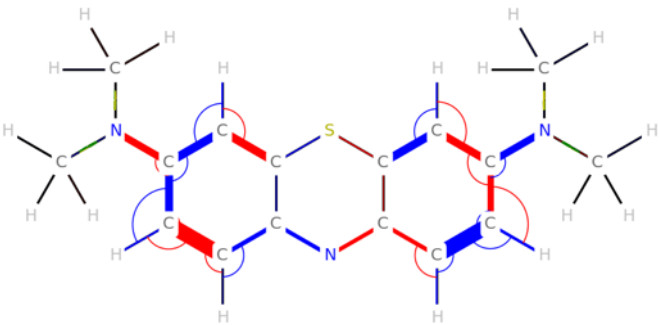
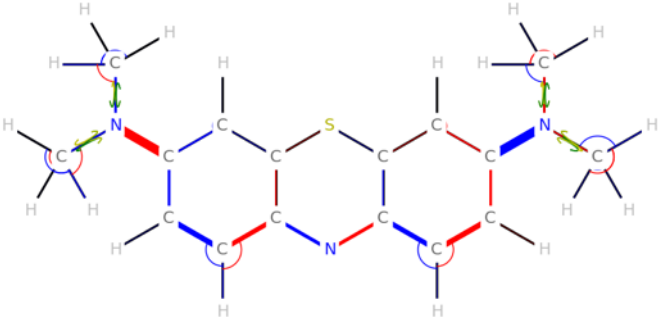


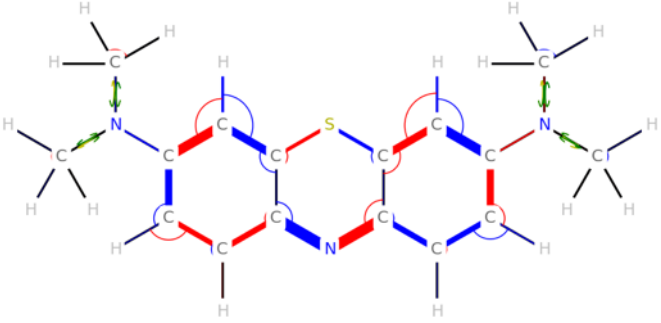
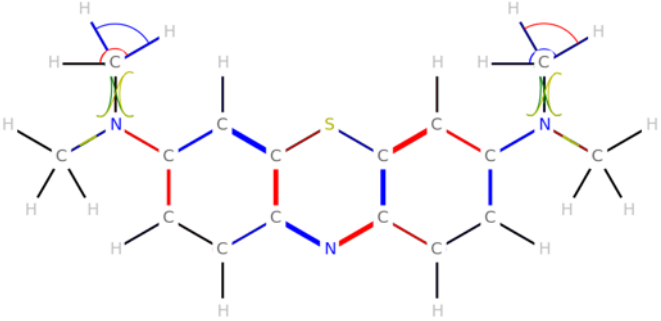
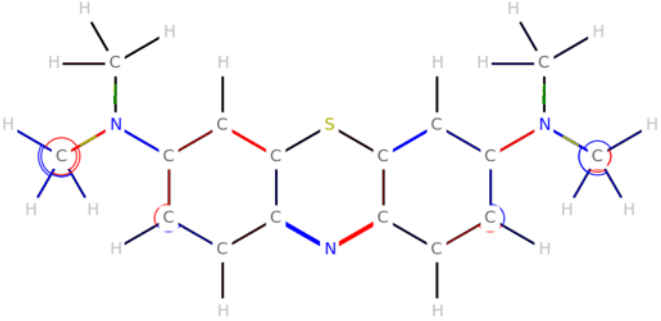
**Figure S6.** Comparison of ATR and DFT-computed spectrum of MB.

In Figure S6, the ATR spectrum recorded (red) and the DFT-computed spectrum (black) are depicted. The DFT calculations match the experimental data with high precision ( $\Delta\nu_{(\text{Exp-DFT})} < \pm 20 \text{ cm}^{-1}$ ). In Table S3, the peak assignment is summarized based on the DFT calculations. Additionally, 2D visualizations of the binding modes are shown as they are obtained from QVibePlot.<sup>1</sup> Note that the direction of the bond movement (stretching or bending) is color-coded in blue and red. Additionally, the width expresses the amplitude of the change in bond length. Finally, deformations out of plane are color-coded in yellow and green. Again, the width correlates with the amplitude of the deformation.

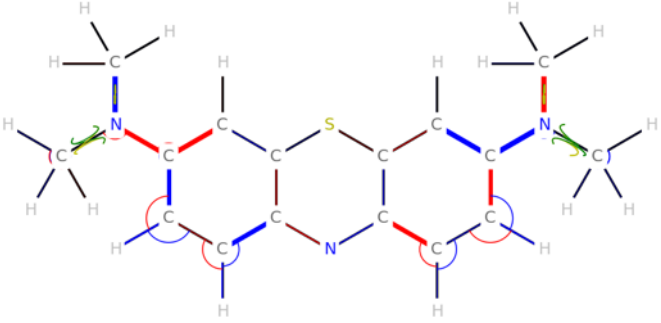
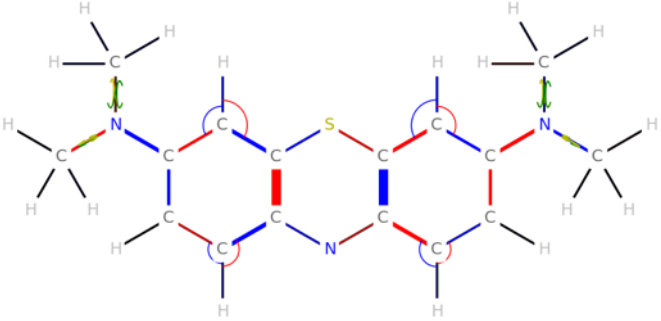
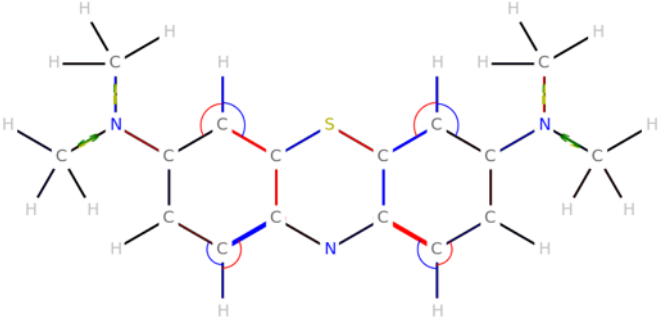
## Peak assignment based on DFT calculation

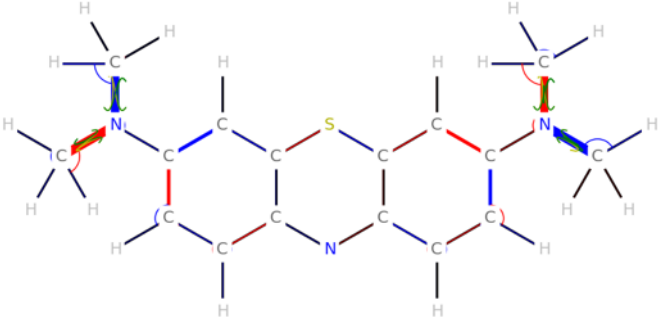
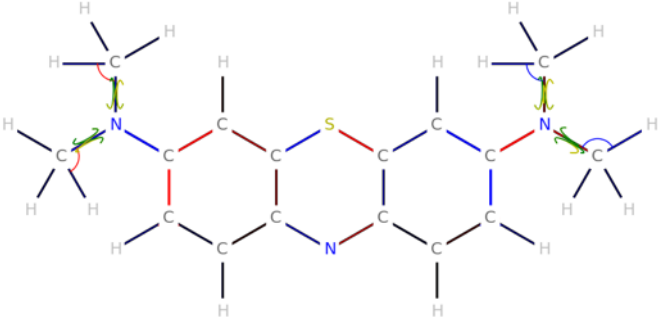
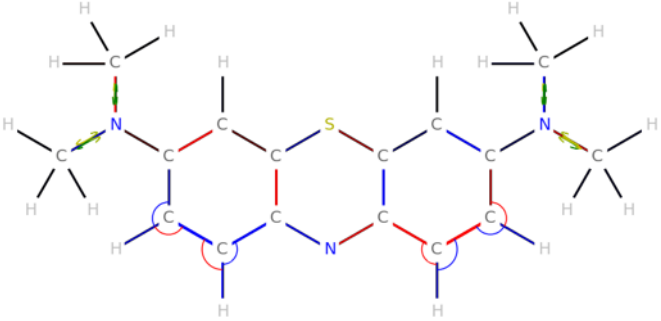
**Table S4.** Peak assignment based on DFT calculation; characteristic MB bands highlighted in yellow.

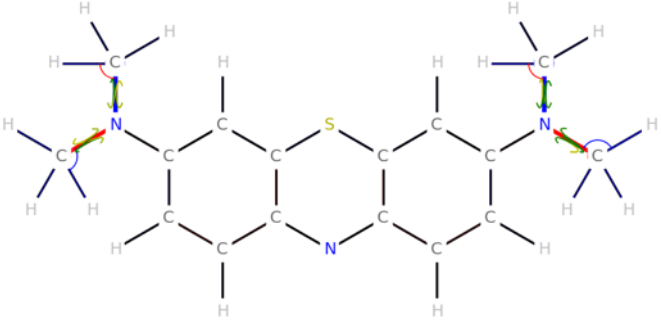
$\nu_{\text{Exp}} / \text{cm}^{-1}$	$\nu_{\text{DFT}} / \text{cm}^{-1}$	$\Delta\nu_{(\text{Exp-DFT})} / \text{cm}^{-1}$	2D Representation via QVibePlot <sup>2</sup>
1593	1596	-3	
1525	1509	16	

1486	1475	11	
1441	1433	8	
1389	1400	-11	



1350	1341	9	 <p>Chemical structure of 1,3-bis(methylamino)thiophene. The structure shows a central thiophene ring with methylamino groups at the 1 and 3 positions. The bonds between the ring carbons and the methylamino nitrogens are highlighted in red and blue. The methyl groups are shown in green.</p>
<b>1331</b>	<b>1325</b>	<b>6</b>	 <p>Chemical structure of 1,3-bis(methylamino)thiophene. The structure shows a central thiophene ring with methylamino groups at the 1 and 3 positions. The bonds between the ring carbons and the methylamino nitrogens are highlighted in red and blue. The methyl groups are shown in green.</p>
1248	1232	16	 <p>Chemical structure of 1,3-bis(methylamino)thiophene. The structure shows a central thiophene ring with methylamino groups at the 1 and 3 positions. The bonds between the ring carbons and the methylamino nitrogens are highlighted in red and blue. The methyl groups are shown in green.</p>

1218	1218	0	
1172	1157	15	
1138	1136	2	

1037	1040	-3	 <p>The image shows the chemical structure of 1,4-dithiane, a six-membered ring with two sulfur atoms at the 1 and 4 positions. The structure is drawn with carbon atoms at the vertices of a hexagon. The sulfur atoms are colored yellow. The nitrogen atoms are colored blue. The hydrogen atoms are colored white. The structure is annotated with stereochemical information: at the 2-position, the C2-S1 bond is shown with a red wedge and a blue dash, and the C2-H2 bond is shown with a green wedge and a blue dash; at the 5-position, the C5-S4 bond is shown with a red wedge and a blue dash, and the C5-H5 bond is shown with a green wedge and a blue dash. The overall structure is a 1,4-dithiane derivative.</p>
------	------	----	--

## Overview of optimized Van der Waals complexes

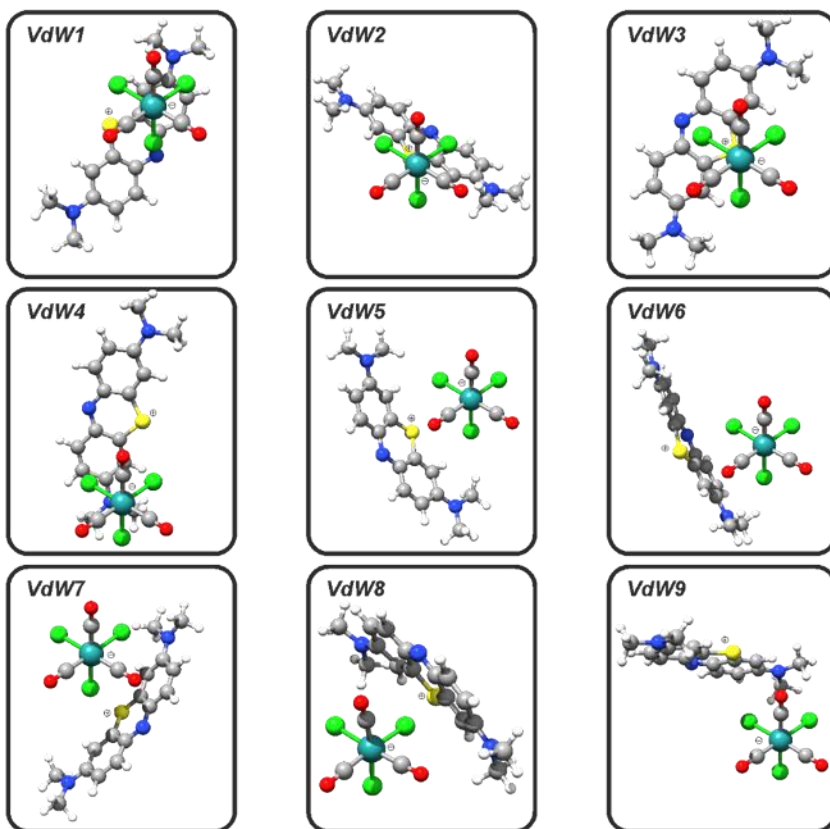
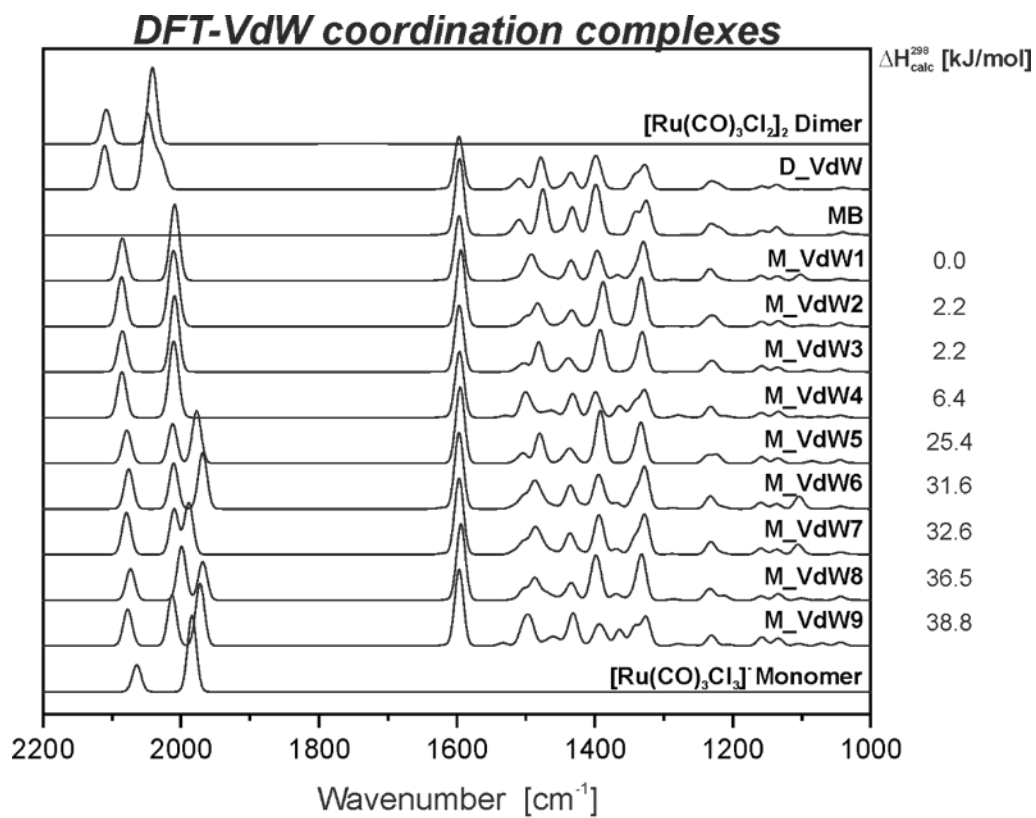


**Figure S7.** Calculated VdW complexes. Relative complexation Enthalpy computed at the BP86-D3/def2-TZVPD level of theory is listed for the monomer complexes referenced against the complex with the lowest energy.

## Illustration of fingerprint region

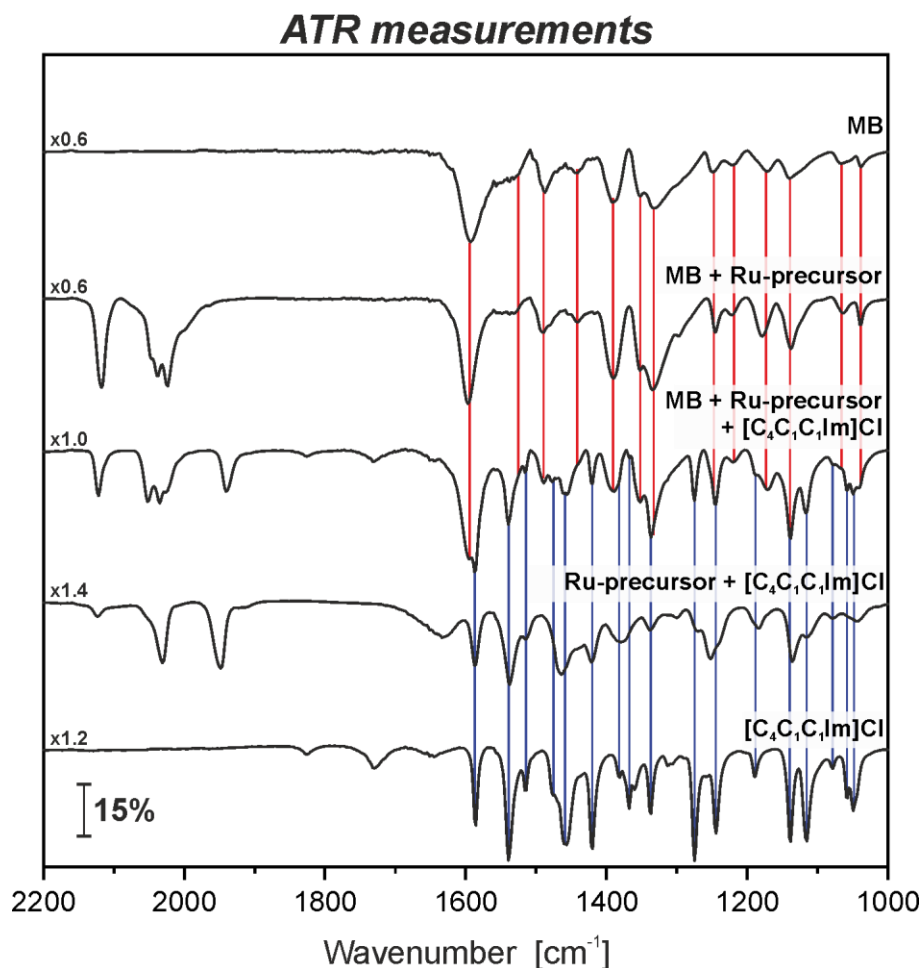


**Figure S8.** ATR fingerprint region.

In Figure S8, the peak positions of the MB and  $[\text{C}_4\text{C}_1\text{C}_1\text{Im}]\text{Cl}$  reference spectra are extended to illustrate whether peaks in the mixtures vanished or shifted to new positions or whether new peaks evolved. However, one can clearly see that there are no changes as compared to the reference spectra.

## **Influence of solvent on DFT calculations**

In the recorded ATR spectra, the CO peak positions do not show a general trend upon addition of MB, i.e. an overall shift to higher or lower wavenumbers. Contrarily, the gas phase DFT spectra of the VdW complexes clearly indicate a shift of the CO band to higher wavenumbers upon addition of MB (Figure 2a). This effect is more pronounced for the charged monomeric species and less for VdW complexes involving the neutral precursor. Since an IL phase is present in the samples investigated experimentally, we reoptimized a subset of the VdW complexes with the SMD-GIL solvation model to estimate the solvent effects of the IL. In Table S4, DFT-computed peak positions are listed to demonstrate the influence of the solvent onto the outcome of the DFT calculations. To that aim, we compare the shifts of the CO peak positions between the free complex and the Van der Waals complex formed ( $\Delta(\text{VdW-Ref})$ ). As one can see, there is basically no peak shift apparent if the calculations include SMD-GIL corrections for  $[\text{C}_4\text{C}_1\text{C}_1\text{Im}]\text{Cl}$ . Contrary, weak shifts are apparent if the calculations are performed in the gas phase. Thus, the general peak shift observed in the gas phase spectra is an effect due to the absence of the solvent.

**Table S5.** Computed  $\nu(\text{CO})$  peak centers of single molecular or coordination complexes with MB. All computations were carried out at the BP86-D3/def2TZPVD level of theory with and without SMD  $[\text{C}_4\text{C}_1\text{C}_1\text{Im}]\text{Cl}$  solvent corrections.

	DFT (CO) peak center [ $\text{cm}^{-1}$ ]				$\Delta(\text{VdW} - \text{Ref})$ [ $\text{cm}^{-1}$ ]			
	$[\text{C}_4\text{C}_1\text{C}_1\text{Im}]\text{Cl}$		Gas-phase		$[\text{C}_4\text{C}_1\text{C}_1\text{Im}]\text{Cl}$		Gas-phase	
<b>Monomer Ref</b>	1982	2080	1984	2064	-	-	-	-
<b>Monomer VdW1</b>	1983	2081	2009	2085	1 <sup>a</sup>	1 <sup>a</sup>	25 <sup>a</sup>	21 <sup>a</sup>
<b>Monomer VdW2</b>	1985	2082	2011	2086	3 <sup>a</sup>	2 <sup>a</sup>	27 <sup>a</sup>	22 <sup>a</sup>
<b>Monomer VdW3</b>	1983	2080	2009	2085	1 <sup>a</sup>	0 <sup>a</sup>	25 <sup>a</sup>	21 <sup>a</sup>
<b>Dimer Ref</b>	2024	2108	2041	2108	-	-	-	-
<b>Dimer VdW</b>	2026	2109	2048	2111	2 <sup>b</sup>	1 <sup>b</sup>	7 <sup>b</sup>	3 <sup>b</sup>

<sup>a</sup> the monomer is used as the reference, <sup>b</sup> the dimer is used as the reference

## Optimized reaction intermediates and transition structures

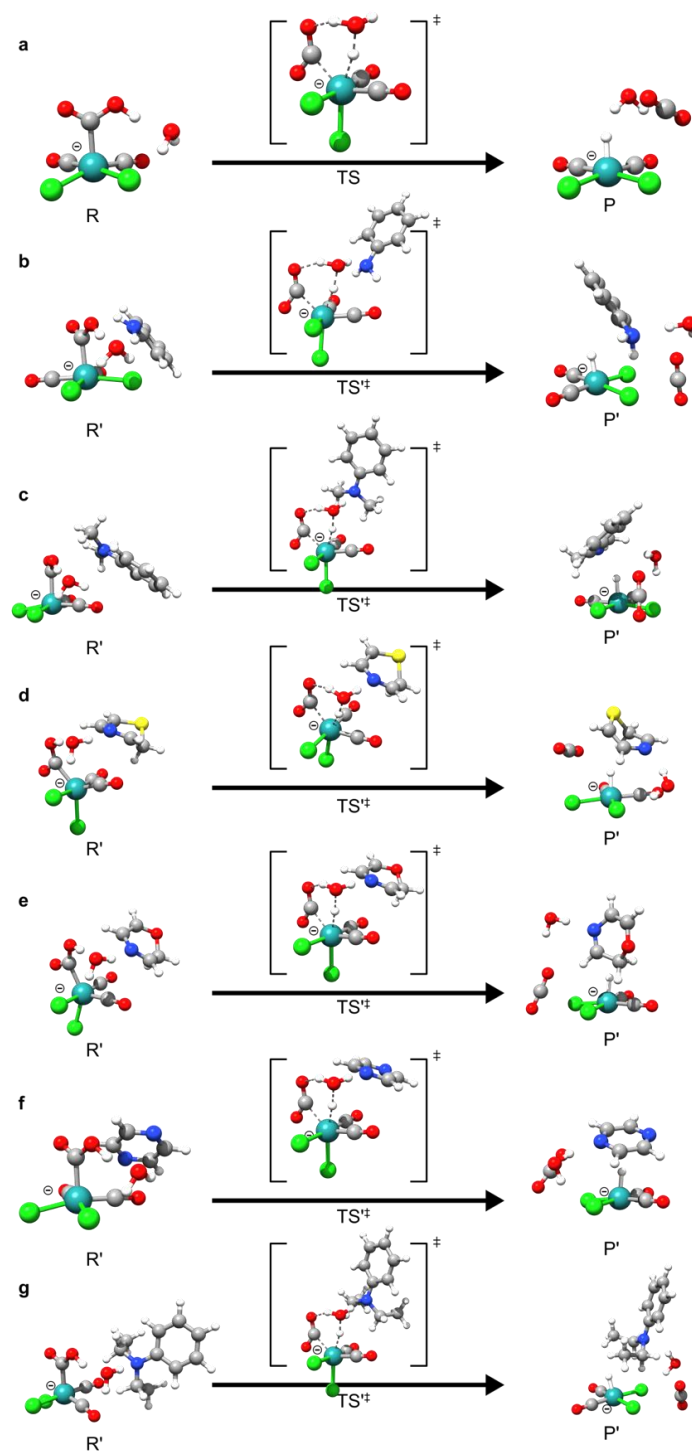


**Figure S9.** Overview of the optimized reactants (R), transition structures (TS) and products (P) for the benchmark without HBA (a) and with the HBAs aniline (b), N,N-dimethylaniline (c), 1,4-thiazine (d), 1,4-oxazine (e), pyrazine (f) and N,N-diethylaniline (g).



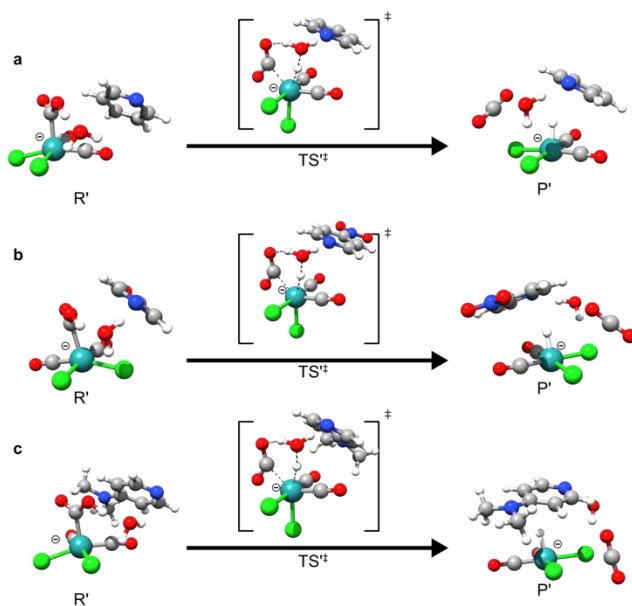


**Figure S10.** Overview of the optimized reactants (R), transition structures (TS) and products (P) with the HBAs pyridine (a), 4-nitro-pyridine (b) and N,N-dimethylpyridine-4-amine (c).

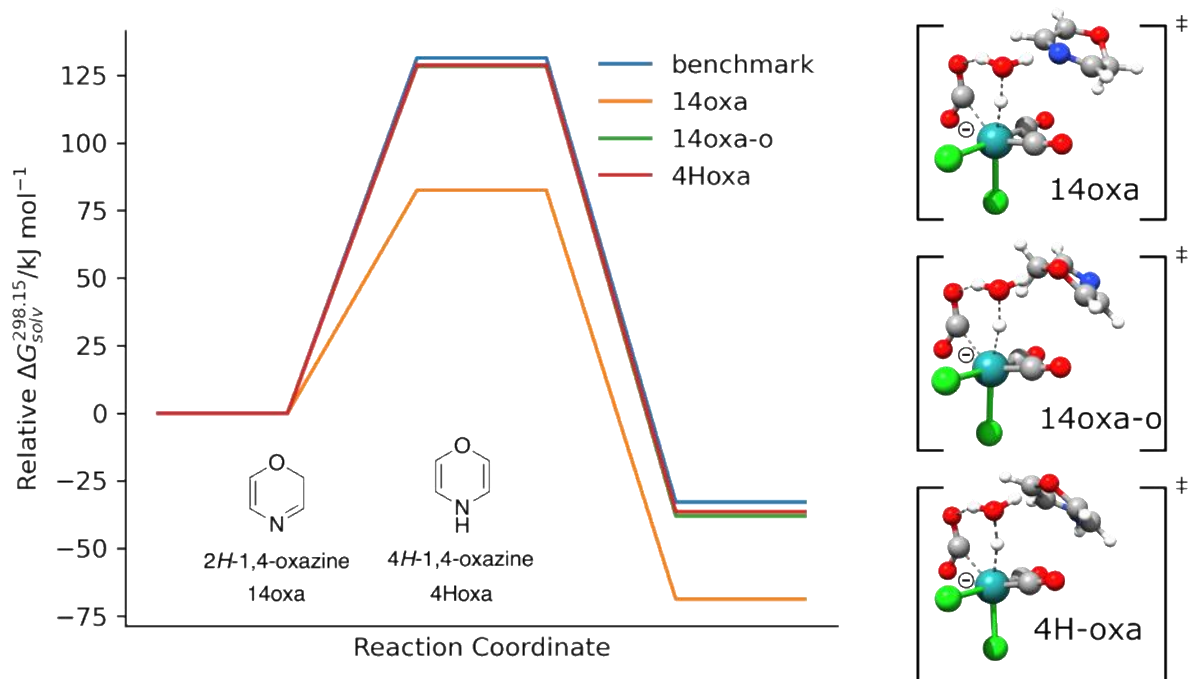


**Figure S11.** Computed barrier heights and free energies of reaction for the rate determining step with and without the effect of oxazines as hydrogen bond acceptors. All energies are computed at the DLPNO-CCSD(T)/def2-TZVPPD // BP86-D3/def2-TZVPD level of theory including SMD-GIL ([C<sub>4</sub>C<sub>1</sub>C<sub>1</sub>Im][Cl]) solvent corrections. The reaction without HBA is delineated as benchmark. The chemical formulas of the HBAs are shown as insets. The reaction energies are calculated relative to the energy of the respective reactant complexes (R).

## Electron density distributions of MB, azure A and thionine chloride

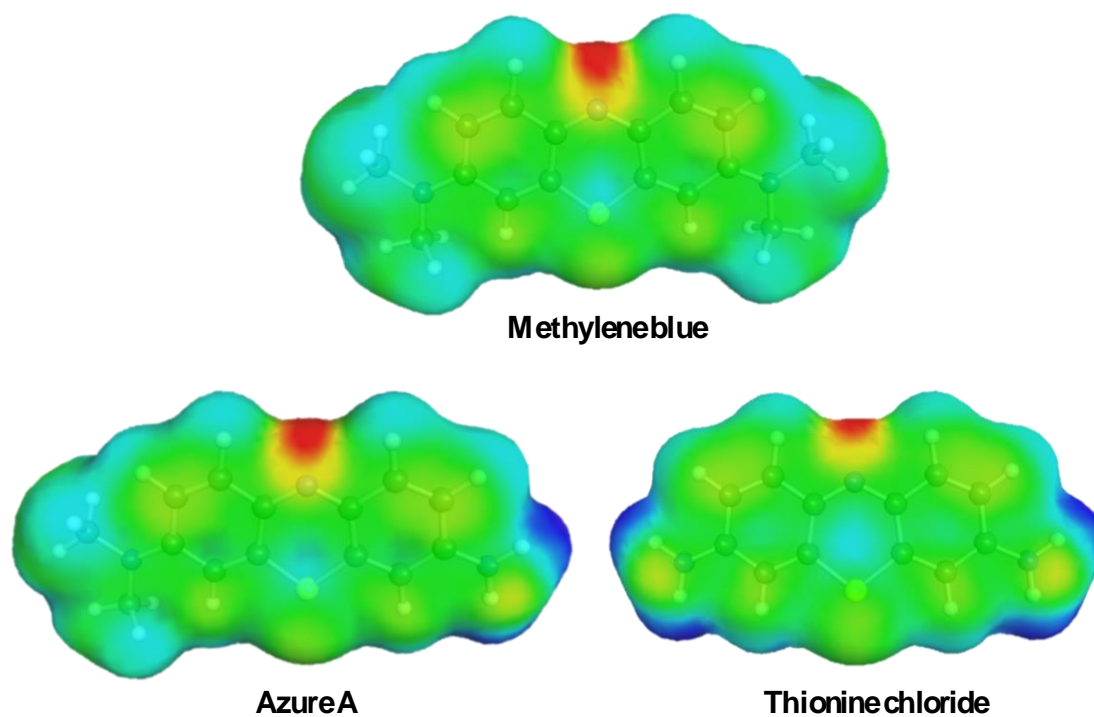


**Figure S12.** Electron density distribution of Methylene blue, Azure A and Thionine chloride. Red-yellow regions show a high electron density while blue regions represent a low electron density. Calculations and image created with COSMOtherm X16.

## Influence of Methylene Green on catalytic activity

To further validate the influence of electron-pushing or electron-withdrawing groups on the catalytic activity, we investigated methylene green (MG), a commercially available molecule with the same basic structure as MB which, however, contains a strongly electron-withdrawing nitro-group (-M-effect). The effects of MG on the catalytic activity are shown in Figure 6.

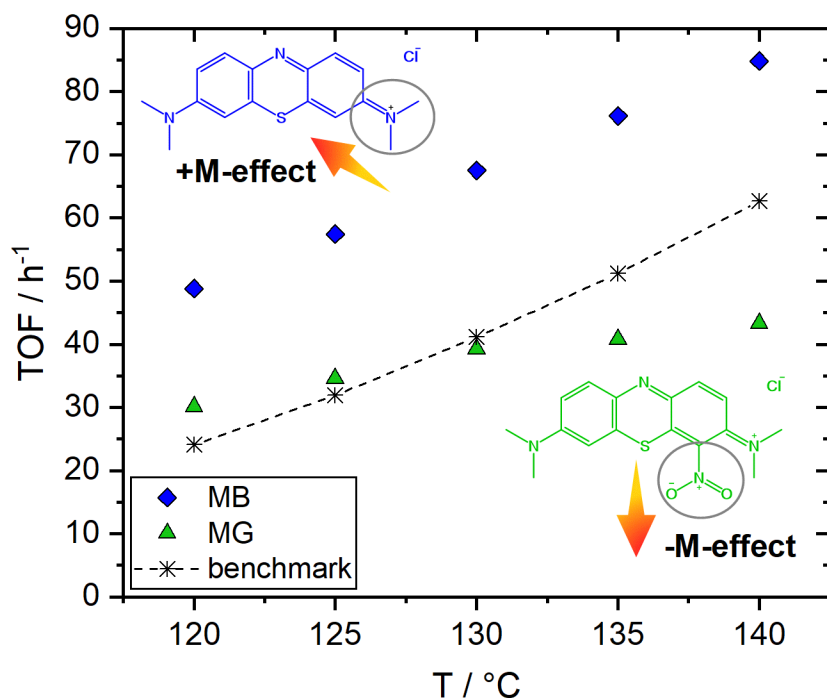


**Figure S13.** Catalytic results of MG compared to MB in the  $[C_4C_1C_1Im]Cl$  film ( $\chi$ ) of the catalyst samples at different temperatures.  $T = 120 - 140$  °C,  $p = 1$  bar, precursor =  $[Ru(CO)_3(Cl)_2]_2$ , loading (Ru) =  $0.02 g g^{-1}_{Support}$ , IL =  $[C_4C_1C_1Im]Cl$ ,  $\alpha = 0.34$ ,  $M_{additive} = 0.5 mol L^{-1}_L$ ,  $m_{cat} = 2.0$  g,  $p_{H_2O}:p_{CO} = 2:1$ ,  $\dot{V}_{tot} = 174 mL_N min^{-1}$ , TOS = 45 h. Maximum error  $\pm 5$  %, error bars omitted for sake of clarity.

As compared to the positive effect upon the addition of MB, MG does have a clear negative influence on the catalytic activity. At 120 °C, the TOF value is already 38 % below the MB-system and further decreases to -50 % at 140 °C. In comparison to the benchmark system, catalysis is still

enhanced upon the addition of MG by +24 % at 120 °C, but this positive effect diminishes with rising temperature. At 130 °C, the activity is 5 % below the benchmark values and continuously decreases to -31 % at 140 °C. Since MB and MG only vary in the additional nitro-group in an outer ring of the molecule, the comparatively low activity of the catalyst system is related to differences in the electron density distribution. Images of the modeled electron density distribution within MG from different perspectives can be found in Figure S14. This analysis clearly shows the formation of a second region with higher electron density besides the central nitrogen atom as expected. This region is located around the electron-withdrawing nitro-group. The second center of high electron density could possibly lower the interaction of the molecule with the active Ru-complex during the catalytic cycle.

## Electron density distribution of Methylene green

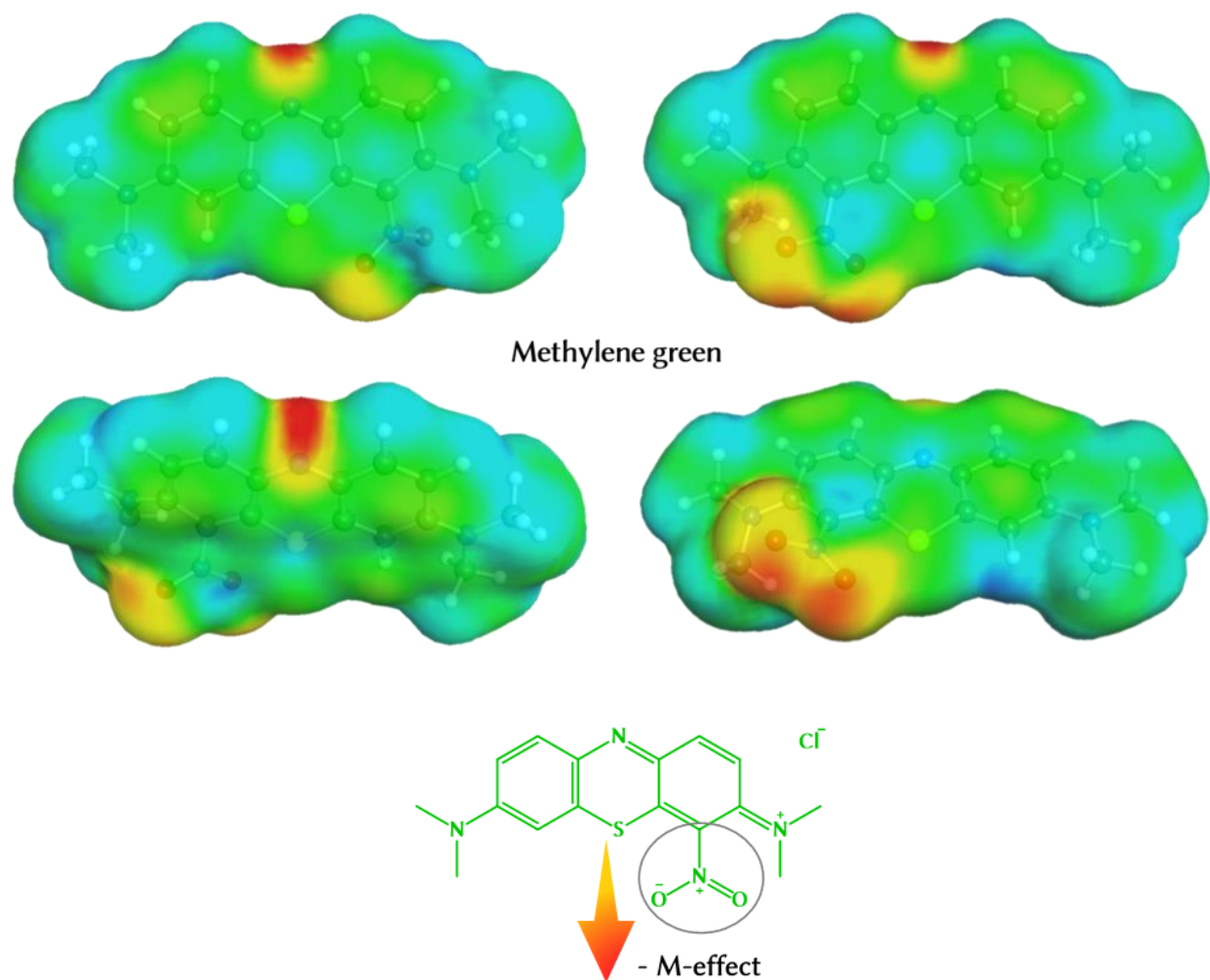


**Figure S14.** Top: electron density distribution within methylene green from different perspectives. Red-yellow shows regions of high electron density while blue regions represent low electron density. Images calculated and created with COSMOtherm X16. Bottom: Methylene Blue (containing two dimethylamino-groups which have a +M-effect) and Methylene Green (carrying additionally a nitro-group which has a –M-effect).

## Methylene blue and some derivatives – differing centered heteroatoms

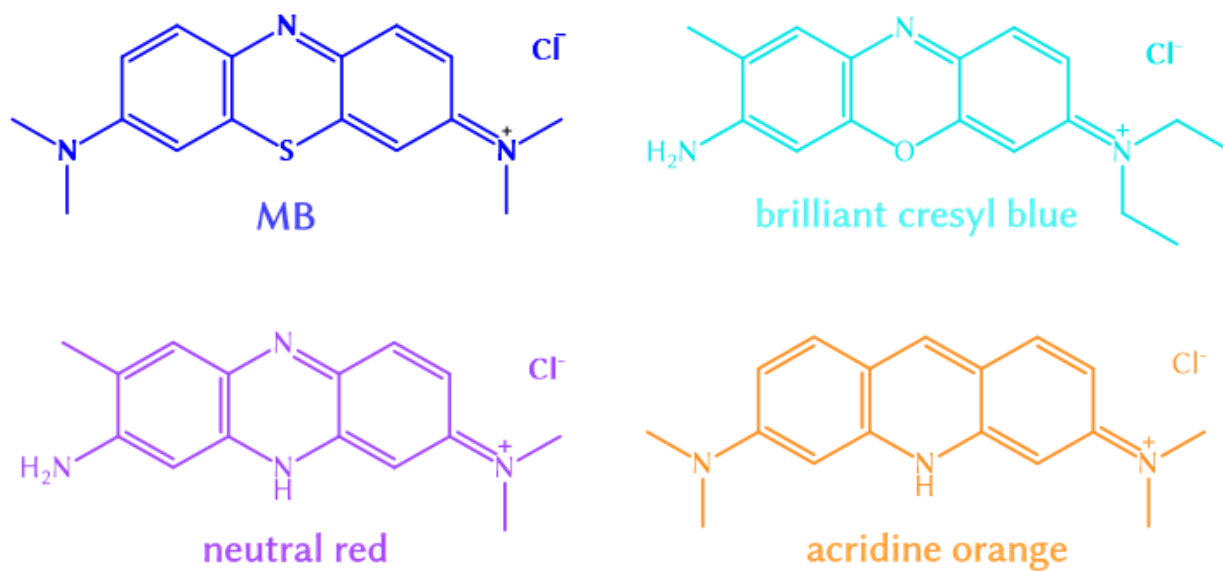


**Figure S15.** Methylene blue and some phenothiazine-based derivatives which differ concerning their central heteroatoms. MB (N and S), brilliant cresyl blue (N and O), neutral red (N and N) and acridine orange (N and C).

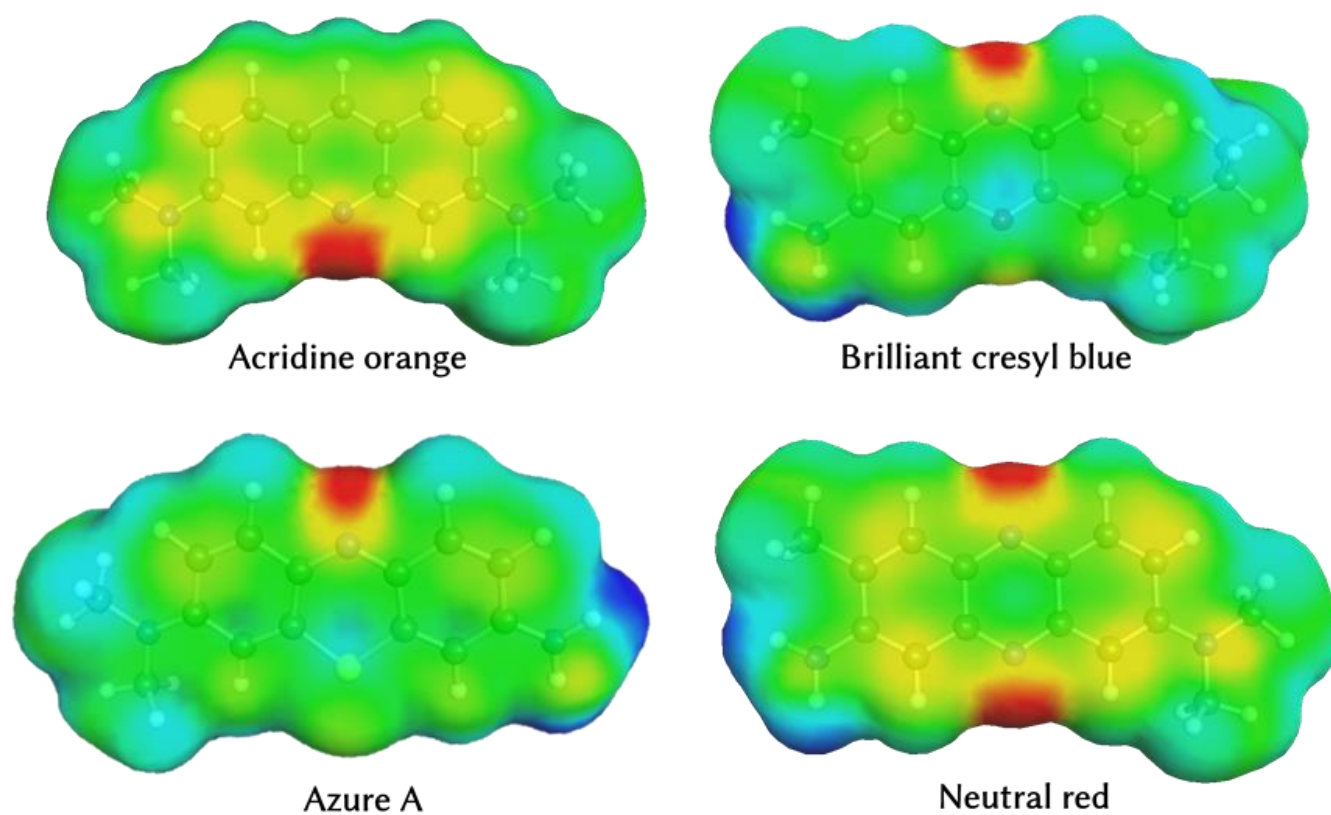


**Figure S16.** Electron density distributions within some phenothiazine-based derivatives which differ concerning their central heteroatoms. Azure A (N and S), Brilliant cresyl blue (N and O), Neutral red (N and N) and Acridine orange (N and C).



## Relationship between the calculated effective barrier and the measured increase of TOF

The theoretical rate constant for the rate determining step can be estimated by the Arrhenius type equation,

$$k = Ae^{\frac{-\Delta G^\ddagger}{RT}} \quad (1)$$

with the rate constant  $k$ , the preexponential factor  $A$ , the energetic barrier  $-\Delta G^\ddagger$ , the gas constant  $R$  and temperature  $T$ . Comparison of the rate constants  $k_{\text{bench}}$  for the benchmark system and the rate constant predicted for an additive  $k_{\text{add}}$  yields (in the logarithmic representation)

$$\ln\left(\frac{k_{\text{add}}}{k_{\text{bench}}}\right) = \frac{-(\Delta G_{\text{add}}^\ddagger - \Delta G_{\text{bench}}^\ddagger)}{RT} = \frac{-\Delta\Delta G^\ddagger}{RT} \quad (2)$$

Replacing the rate constants by the measured TOF, which directly reflects the catalytic activity, we can expect a linear relationship between the theoretical barrier and the measured TOF according to equation 2.

## Literature

1. Bauer T, Stepic R, Wolf P, Kollhoff F, Karawacka W, Wick CR, *et al.* Dynamic equilibria in supported ionic liquid phase (SILP) catalysis: in situ IR spectroscopy identifies  $[\text{Ru}(\text{CO})_x\text{Cly}]_n$  species in water gas shift catalysis. *Catalysis Science & Technology* 2018, **8**(1): 344-357.
2. Laurin, M. QVibepplot: A Program to Visualize Molecular Vibrations in Two Dimensions. *J. Chem. Educ.* 2013, 90(7): 944-946